Endothelial exocytosis of angiopoietin-2 resulting from CCM3 deficiency contributes to cerebral cavernous malformation

Huanjiao Jenny Zhou[1,2,11], Lingfeng Qin[1,11], Haifeng Zhang[1,11], Wenwen Tang[1,3], Weidong Ji[2,4], Yun He[1,5], Xiaoling Liang[6], Zongren Wang[2], Qianying Yuan[1,3], Alexander Vortmeyer[1], Derek Toomre[7], Germaine Fuh[8], Minghong Yan[9], Martin S Kluger[1,10], Dianqing Wu[1,3] & Wang Min[1,2,4]

Cerebral cavernous malformations (CCMs) are vascular malformations that affect the central nervous system and result in cerebral hemorrhage, seizure and stroke. CCMs arise from loss-of-function mutations in one of three genes: *KRIT1* (also known as *CCM1*), *CCM2* or *PDCD10* (also known as *CCM3*). *PDCD10* mutations in humans often result in a more severe form of the disease relative to mutations in the other two CCM genes, and *PDCD10*-knockout mice show severe defects, the mechanistic basis for which is unclear. We have recently reported that CCM3 regulates exocytosis mediated by the UNC13 family of exocytic regulatory proteins. Here, in investigating the role of endothelial cell exocytosis in CCM disease progression, we found that CCM3 suppresses UNC13B- and vesicle-associated membrane protein 3 (VAMP3)-dependent exocytosis of angiopoietin 2 (ANGPT2) in brain endothelial cells. CCM3 deficiency in endothelial cells augments the exocytosis and secretion of ANGPT2, which is associated with destabilized endothelial cell junctions, enlarged lumen formation and endothelial cell–pericyte dissociation. UNC13B deficiency, which blunts ANGPT2 secretion from endothelial cells, or treatment with an ANGPT2-neutralizing antibody normalizes the defects in the brain and retina caused by endothelial-cell-specific CCM3 deficiency, including the disruption of endothelial cell junctions, vessel dilation and pericyte dissociation. Thus, enhanced secretion of ANGPT2 in endothelial cells contributes to the progression of CCM disease, providing a new therapeutic approach for treating this devastating pathology.

CCMs consist of clusters of enlarged endothelial channels ('caverns') that are arranged back to back to form densely packed sinusoids with little or no intervening brain parenchyma[1,2]. These lesions lack pericytes and elastic tissue, such that the vessel walls are thin, leaky and lack subendothelial support and an intact basal lamina. As compared to normal vessels, ultrastructural analysis of CCM lesions has revealed a decreased number of perictyes, endothelial detachment from the basal lamina and ruptures in the luminal endothelium, probably because of reduced and/or damaged intercellular junctions[3]. CCMs are found almost exclusively in the neurovasculature of the central nervous system (CNS, i.e., brain and retina)[4,5], and they result in an increased risk for stroke, seizures and focal neurological deficits[1,2]. Currently, the only treatment for CCM is surgical resection.

CCMs can be sporadic or familial. More than 90% of people with inherited autosomal-dominant CCMs carry loss-of-function mutations in one of three genes: *KRIT1* (encoding CCM1)[6], *CCM2* (ref. 7) or *PDCD10* (encoding CCM3)[8]. CCM has been thought to result from a 'two-hit' mechanism; in individuals who carry one mutated allele of one of the CCM genes in the germline, a somatic mutation at the second allele has been identified in endothelial cells lining cavernous vessels[9–11]. This finding has been confirmed recently in a mouse model[12]. In mice, postnatal inactivation of CCM genes in endothelial cells induces brain CCM lesions that are characterized by a single layer of dilated endothelium, closely resembling human CCM[13–17]. Similarly to human CCM, knockout of any one of the CCM genes in mice produces CCM, which suggests that the three proteins function in a common pathway. In accordance with this hypothesis, all three proteins can be found in the same complex within the cell, and they mediate several shared signaling pathways[16,18–20]. However, CCM3 might also act separately from CCM1 and CCM2, as *PDCD10* mutation often results in a more severe form of the disease[21], and *Pdcd10*-knockout mice show severe defects, resulting from yet-to-be defined mechanisms[13–17].

CCM3 associates with the germinal center kinase III (GCKIII) kinases (including STK24 and STK25), and these kinases function in

---

the same pathway as CCM3 in cardiovascular development[22,23]. We recently found that CCM3 and STK24 negatively regulate exocytosis[24], a process wherein a cell directs the contents of secretory vesicles toward the extracellular space. These membrane-bound vesicles contain soluble proteins to be secreted into the extracellular environment and membrane proteins and lipids to be incorporated into the cell membrane. The size and contents of exocytic vesicles (also called granules) vary, and these characteristics are highly cell-type dependent. Exocytosis is accomplished by the fusion of secretory vesicles with the plasma membrane through the assembly of the soluble N-ethylmaleimide-sensitive factor (NSF) attachment protein receptor (SNARE) complex. Before membrane fusion, additional proteins mediate and regulate the initial interaction between vesicles and the acceptor membrane. These proteins include the plasma membrane proteins syntaxins; synaptosomal-associated proteins (SNAPs); vesicle-associated membrane proteins (VAMPs); the Rab family of small GTPases; the exocyst; and numerous other regulatory proteins. Among these regulatory proteins is the UNC13 family, which consists of UNC13A–D (ref. 25). UNC13B and UNC13D contain two separate Ca^{2+}-binding C2 domains (C2A and C2B), and both UNC13B and UNC13D are involved in the tethering of granules to plasma membranes through the binding of their C2B domains to membrane lipids during granule docking and priming, before vesicle fusion with the plasma membrane. Our previous mechanistic studies suggested that

CCM3 and STK24, by inhibiting UNC13 family proteins, regulate exocytosis and neutrophil degranulation[24].

The exocytic machinery that drives vesicle trafficking and membrane fusion in endothelial cells is similar to that found in neurons and neutrophils[26]. Endothelial cells contain the Weibel–Palade body (WPB), a type of secretory vesicle that releases von Willebrand factor (vWF) and P-selectin during inflammation. Moreover, ANGPT2 is released from WPBs in endothelial cells[27,28]. ANGPTs (ANGPT1 and ANGPT2) are endothelial growth factors that bind to the tyrosine kinase receptor TIE2 (encoded by *Tek*), cooperatively regulating endothelial cell adherens junction-dependent vascular stability and blood-vessel formation during angiogenesis[29].

In the present study, our observation that ANGPT2 levels are increased in both mouse and human CCM lesions prompted us to explore the role of the CCM3–UNC13 network in the regulation of the release of ANGPT2 and the implications of this regulation for CCM lesion development.

RESULTS

Mice with endothelial-cell-inducible *Pdcd10* deletion develop CCM lesions

To obtain mice with tamoxifen-inducible, endothelial-specific deficiency of CCM3, we used *Cdh5-CreERT2;Pdcd10*^{fl/fl} mice (hereafter termed *Pdcd10*[ECKO] mice). We first documented that the Cdh5-CreERT2 allele drove tamoxifen-inducible, endothelial-specific expression by mating *Cdh5-CreERT2* mice with *mT/mG*-reporter mice. Feeding tamoxifen to *Cdh5-CreERT2;mT/mG* pups from postnatal (P)1 to P3 resulted in the induction of mG (EGFP) expression specifically in the vasculature of multiple tissues, including brain (**Supplementary Fig. 1a**). Next, we induced endothelial-cell-specific deletion of *Pdcd10* in *Pdcd10*[ECKO] pups immediately after birth (**Supplementary Fig. 1b,c**). *Pdcd10*[ECKO], but not wild-type (WT) (*Pdcd10*^{fl/fl}) pups, rapidly developed CCM lesions with dilated capillaries in the cerebellum, with onset at P5 and large lesions evident at P10 (**Fig. 1a**). No *Pdcd10*[ECKO] pups survived beyond P15 ($n > 50$). CCM lesions (>10,000 μm^2) were detected primarily inside the granule cell layers of the cerebellum of *Pdcd10*[ECKO] mice, and lesion size was greatly enlarged at P10, as compared to P5 (**Fig. 1a–c**). CCM lesions in humans are formed by enlarged and irregular blood vessels
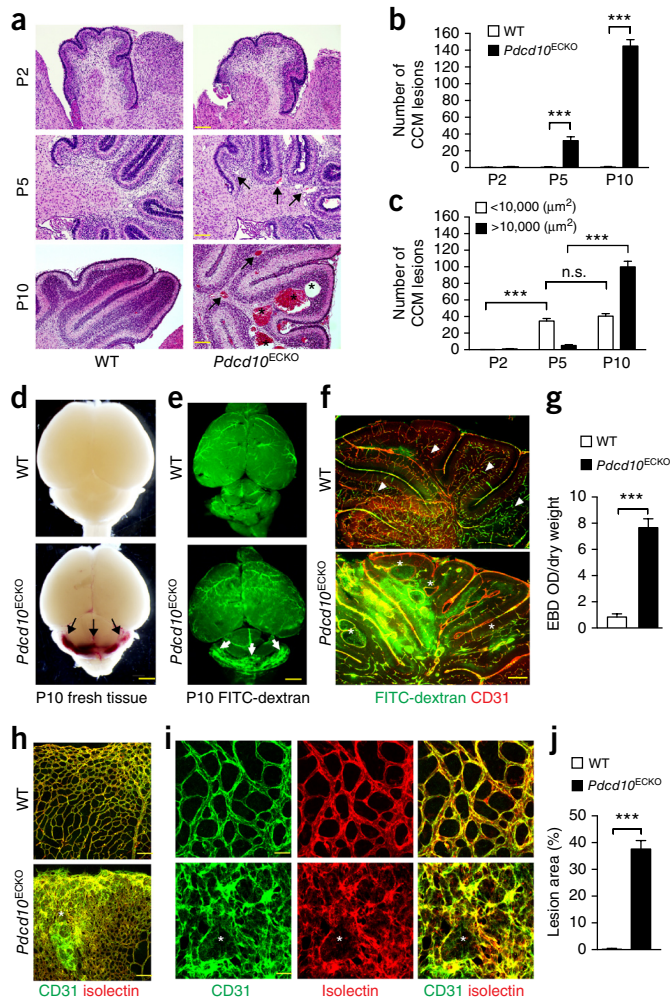

Figure 1 Endothelial-cell-inducible *Pdcd10* deletion (*Pdcd10*[ECKO]) mice develop CCM lesions. (**a–c**) CCM lesion quantification in WT (*Pdcd10*^{fl/fl}) and *Pdcd10*[ECKO] (*Cdh5-CreERT2;Pdcd10*^{fl/fl}) mice. (**a**) H&E staining of cerebellum sections at the indicated ages. Representative images of small lesions (arrows) and large lesions (asterisks) are shown. The number of total lesions (**b**) and small and large lesions (**c**) in *Pdcd10*[ECKO] mice were quantified ($n = 10$ mice). n.s., not significant. ***$P < 0.001$ (two-way ANOVA). (**d–g**) Vascular leakage in CCM lesions. (**d**) Images of fresh brain tissue from WT and *Pdcd10*[ECKO] mice at P10. (**e,f**) Vascular leakage in P10 pups, as assessed by perfusion with FITC-dextran (2,000 kDa) (**e**, arrows point to sites of leakage) and immunostaining of brain sections with anti-CD31 (**f**, asterisks indicate CCM lesions in *Pdcd10*[ECKO] mice; arrowheads indicate a normal granule cell layer in each lobule of the cerebellum in WT mice). (**g**) Cerebellum permeability, as assessed by Evans blue-dye (EBD) assay in WT and *Pdcd10*[ECKO] mice ($n = 10$ mice per group). ***$P < 0.001$ (unpaired two-tailed Student's t test). OD, optical density. (**h,i**). Lesions in retinas. Retinas from P10 WT and *Pdcd10*[ECKO] pups were stained with the endothelial cell markers CD31 (green) and isolectin B4 (red). Asterisks indicate CCM lesions with a disorganized vasculature in confocal images of **h** (20×) and **i** (80×). (**j**) Quantification of lesion areas (% of total retina). $n = 10$ mice per group. ***$P < 0.001$ (unpaired two-tailed Student's t test). Values are means ± s.e.m. Scale bars, 400 μm (**a**); 100 μm (**f,h**); 2 mm (**d,e**); 25 μm (**i**).
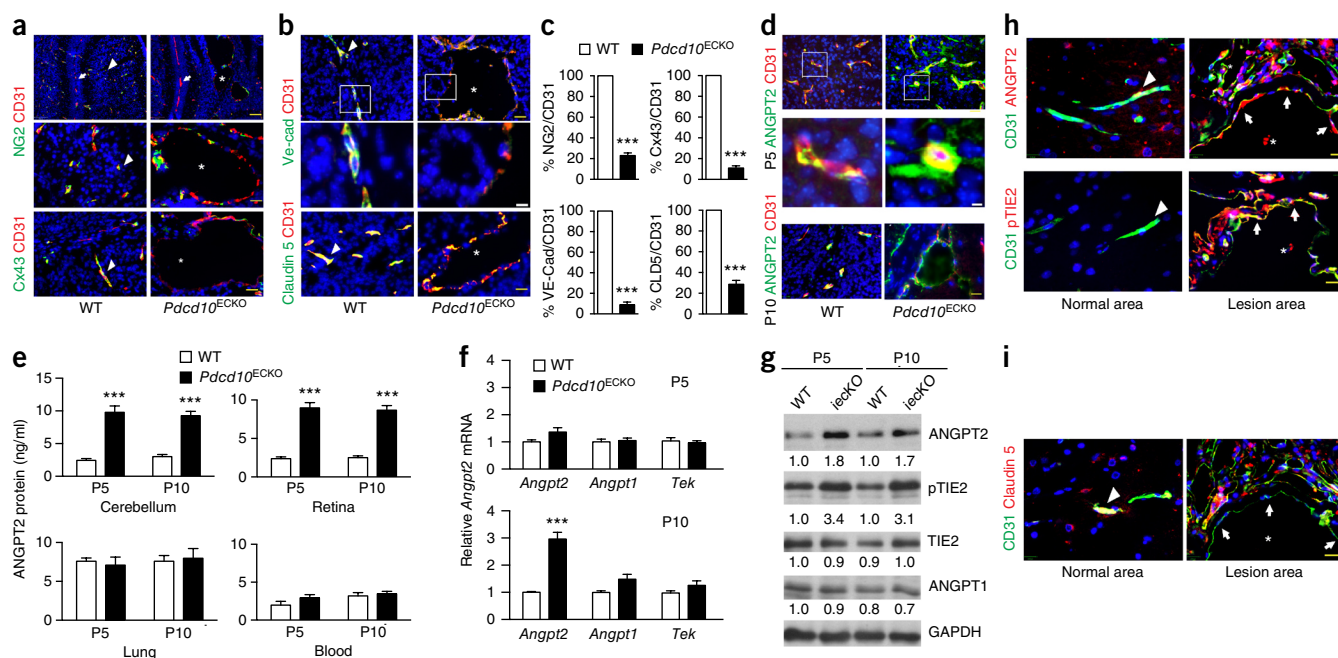
Figure 2 *Pdcd10*^ECKO mice exhibit disrupted endothelial cell–pericyte and endothelial cell–endothelial cell junctions with increased ANGPT2 levels. (**a**) Cerebellum sections from P10 WT and *Pdcd10*^ECKO mice co-stained for CD31 with NG2 (top row, 10×; middle row, 40×) and CD31 with connexin 43 (Cx43). (**b**) Cerebellum sections from P10 WT and *Pdcd10*^ECKO mice co-stained for CD31 and VE-cadherin (Ve-cad) or CD31 with claudin 5. The boxed areas are shown at high power for VE-cadherin and CD31 staining. In **a** and **b**, representative images of normal vessels (arrowheads), CCM lesions (asterisks) and vessels between lobules (arrows) are shown. (**c**) Quantification of co-staining of NG2, Cx43, VE-cadherin and claudin 5 (CLD5) on CD31-positive vessels from P10 WT and *Pdcd10*^ECKO mice. (**d**) Cerebellum sections of P5 and P10 WT and *Pdcd10*^ECKO mice co-stained for ANGPT2 and CD31. The boxed areas, showing representative images of ANGPT2-positive vessels, are shown at high power. (**e**) ANGPT2 protein levels, determined by ELISA, in cerebellum, retinal and lung tissues, as well as blood from P5 and P10 WT and *Pdcd10*^ECKO pups. (**f,g**) mRNA levels (**f**) and protein levels (**g**) of the indicated proteins involved in angiopoietin–TIE2 signaling in the cerebellum of P5 and P10 WT and *Pdcd10*^ECKO pups were determined by RT-qPCR and western blotting. Data represent fold changes compared to WT levels. iecKO, *Pdcd10*^ECKO. *n* = 10 mice per group in **a**–**g**, ***P < 0.001 (unpaired two-tailed Student's *t* test). Values are means ± s.e.m. (**h,i**) Co-staining of CD31 with ANGPT2 or pTIE2 (**h**) or co-staining of CD31 with claudin 5 (**i**) in human CCM specimens. Normal and lesion areas are indicated. Representative images from one of eight cases (case #2) of CCM from individuals with *PDCD10* mutations are shown. Arrowheads indicate normal vessels; asterisks indicate lesions; arrows indicate ANGPT2 or pTIE2 staining (**h**) and loss of claudin 5 staining (**i**) in lesions. Scale bar, 100 μm (**a**, top row); 25 μm (yellow in **a,b,d,h** and **i**); 5 μm (white for boxed images in **b** and **d**).

that often result in cerebral hemorrhage. FITC-dextran perfusion at P10 showed that FITC-dextran was constrained inside the capillary beds of the brains and retina in WT mice, but was diffused to surrounding tissues in the cerebellum of *Pdcd10*^ECKO mice (**Fig. 1d–f**). Evans blue-dye permeability assay also showed increased vascular leakage in the cerebellum of *Pdcd10*^ECKO mice, as compared to WT mice (**Fig. 1g**). Venous malformations were also detected at the periphery of the retinal vascular plexus (**Fig. 1h–j**), but not in skin or liver, as visualized by isolectin and CD31 staining. The retina in *Pdcd10*^ECKO mice was leaky, as indicated by hemorrhage in freshly isolated retinas and by visualization using a FITC-dextran perfusion assay (**Supplementary Fig. 2a,b**).

CCM lesions exhibit disrupted endothelial cell junctions with increased ANGPT2 expression

To study the mechanisms responsible for capillary enlargement in *Pdcd10*^ECKO mice, we examined endothelial cell junctions and endothelial cell–periocyte interactions within the lesions. The lesions in *Pdcd10*^ECKO mice were characterized by a single layer of dilated endothelium with significantly reduced pericyte coverage, as seen in human CCM lesions (**Fig. 2a**). Endothelial cell–pericyte association, as visualized by gap junctional protein connexin 43 staining, was also drastically attenuated in CCM lesions relative to normal vessels (**Fig. 2a**). Endothelial adherens junctions, as visualized by

VE-cadherin staining, were disorganized and were markedly fewer in number in lesion areas, as compared to normal vessels in the brains of WT mice (**Fig. 2b**). Similarly, tight junction coverage in lesions, as visualized by claudin 5 staining, was also drastically reduced (**Fig. 2b**). Quantitation analyses showed significant reductions of pericytes and the three types of cell junction within CCM lesions, as compared to normal microvessels (**Fig. 2c**). ANGPT2, secreted by endothelial cells, is classically considered to be an ANGPT1 antagonist, counteracting the stabilizing action of ANGPT1 and thereby increasing endothelial cell permeability[30,31]. Although ANGPT2 was detected in the endothelial cells of normal vessels in the brains of WT mice, ANGPT2 levels were highly upregulated in the brain of *Pdcd10*^ECKO mice, both inside the dilated vessels and outside the lesions (**Fig. 2d**). ANGPT2 protein levels, as detected by ELISA, were highly increased in the cerebellum of *Pdcd10*^ECKO mice, as compared to WT mice. We also detected increased ANGPT2 levels in the retina, but not in lung tissue or blood (**Fig. 2e**), which is consistent with the location of the lesions. The expression of *Angpt2* mRNA (but not of *Angpt1* or *Tek* (also known as *Tie2*) mRNA) was increased weakly at P5 and strongly at P10 in the cerebellum of *Pdcd10*^ECKO mice (**Fig. 2f**). Unexpectedly, we detected increased levels of TIE2 phosphorylation in *Pdcd10*^ECKO brains, as assessed by western blotting (**Fig. 2g**), which suggests the activation of ANGPT2–TIE2 signaling during CCM lesion development.
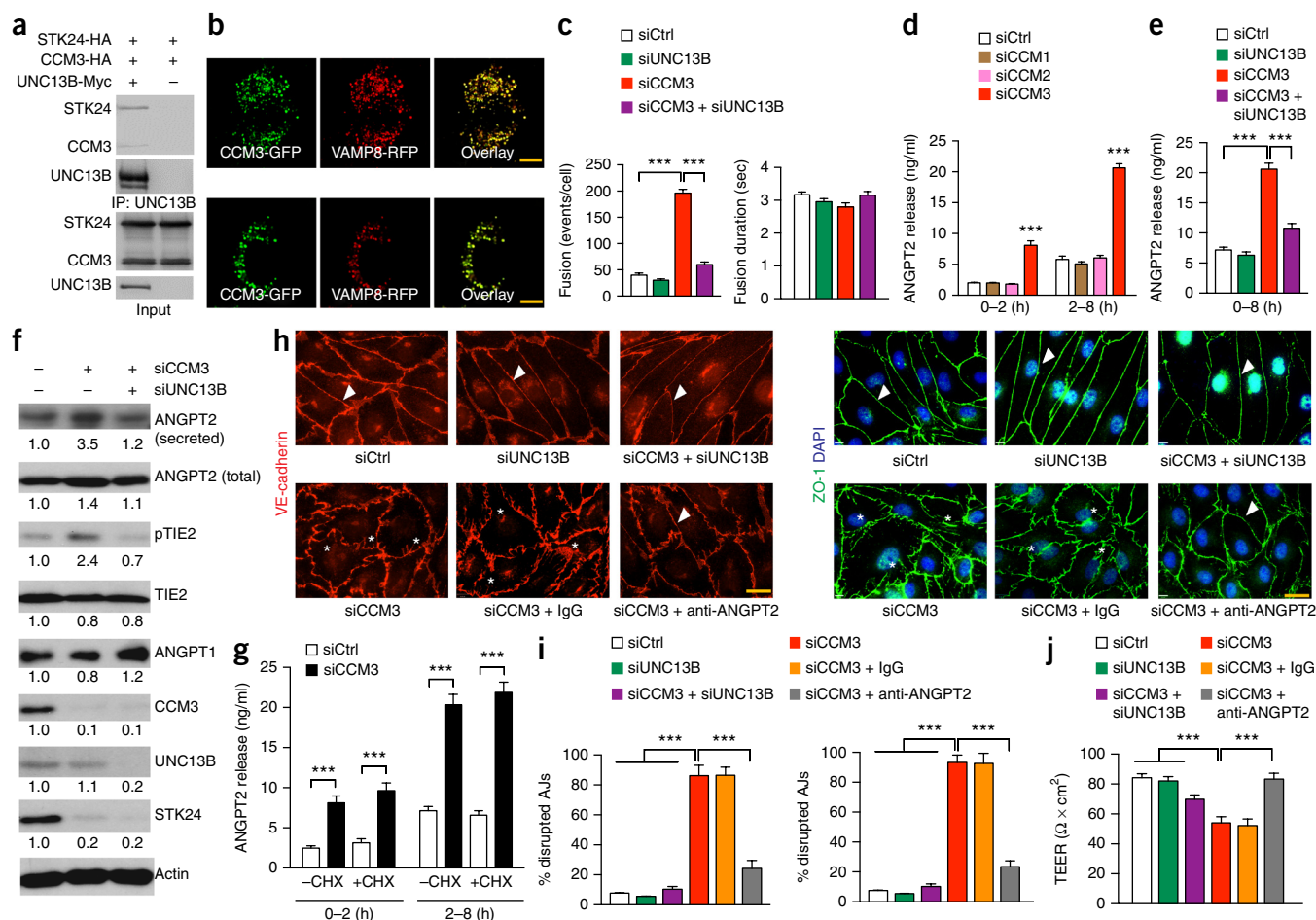
Figure 3 CCM3 restrains ANGPT2 release from endothelial cells and maintains endothelial junctions. (**a**) The association of UNC13B with CCM3 and STK24 in human embryonic kidney (HEK)293T cells transfected with the indicated constructs was determined by immunoprecipitation (IP) with anti-Myc antibody (UNC13B), followed by western blotting with anti-HA antibody (CCM3 and STK24). (**b**) Co-localization of CCM3-GFP and VAMP8-RFP or VAMP3-RFP expressed in HBMVECs after transient transfection. Representative images are shown for one of ten cells examined. (**c**) Fusion events per cell and fusion duration in HBMVECs after transient transfection with the indicated siRNAs. $n = 10$, ***$P < 0.001$ (one-way ANOVA). (**d**–**g**) Secreted ANGPT2 levels in culture media (**d**,**e**,**g**, as determined by ELISA), secreted ANGPT2, intracellular ANGPT2 and other indicated proteins (**f**, as determined by western blotting) from HBMVECs transfected with the indicated siRNAs for 72 h. The transfected cells were replenished with fresh media without (**d**,**e**,**f**) or with CHX (**g**). ANGPT2 levels that accumulate in the media between 0 and 2 h; 2 and 8 h; and 0 and 8 h were measured. Data in panel **f** represent fold changes, as compared to control siRNA. $n = 6$, ***$P < 0.01$ (two-way ANOVA in **d** and **g**; one-way ANOVA in **e**). (**h**) Endothelial adherens junctions and tight junctions were visualized by immunostaining with VE-cadherin and ZO-1, respectively, in HBMVECs treated with a control IgG or ANGPT2 neutralizing antibody (10 μg/ml) 16 h after transfection with siCCM3. (**i**) Percentages of disrupted adherens junctions (AJs) and tight junctions (TJs) (100 microscope fields were counted for each group). (**j**) Barrier function of HBMVECs cultured on fibronectin-coated ECIS cultureware was evaluated using transendothelial electric resistance (TEER; expressed as Ohms (Ω) multiplied by cm^2) by electrical cell-substrate impedance sensing. $n = 12$ wells per group. ***$P < 0.001$ (one-way ANOVA). All experiments were repeated twice. Values are means ± s.e.m. Scale bars, 20 μm (**b**,**h**).

To determine whether ANGPT2 upregulation has clinical relevance, we examined the expression of ANGPT2 in human CCM3 lesions. We obtained paraffin blocks for eight cases of human CCM3 lesions. Six of the samples contained typical CCM lesions surrounded by relatively normal tissue, according to H&E staining, whereas the other two cases had severe vascular fibrosis (**Supplementary Fig. 3a**). ANGPT2 and pTIE2 staining was absent in normal brain areas, but was significantly upregulated in the CCM lesions of all eight cases, accompanied by the disruption of endothelial junctions (**Fig. 2h,i**; **Supplementary Fig. 3b–e**).

CCM3 restrains ANGPT2 secretion and maintains endothelial cell junctions

To determine whether CCM3 regulates ANGPT2 secretion via UNC13-dependent exocytosis in vascular endothelial cells, we first examined the expression of UNC13 family members in both mouse and human brain microvascular endothelial cells (MBMVECs and HBMVECs, respectively). UNC13B was the UNC13 isoform expressed predominantly, as detected by RT–qPCR (**Supplementary Fig. 4a,b**). Moreover, we found that UNC13B forms a complex with CCM3 and the GCKIII family member STK24 (**Fig. 3a**), and that CCM3 co-localized with the vesicle-associated membrane proteins VAMP3 and VAMP8 in HBMVECs (**Fig. 3b**). To determine directly whether CCM3 regulates exocytosis in endothelial cells, we used VAMP8 fused to the pH-sensitive fluorescent protein PHluorin to visualize fusion processes of individual exocytic vesicles, as imaged using live-cell TIRF microscopy. HBMVECs were co-transfected with the PHluorin probe and a control short interfering (si)RNA or CCM3 siRNA in the presence or absence of an UNC13B siRNA.
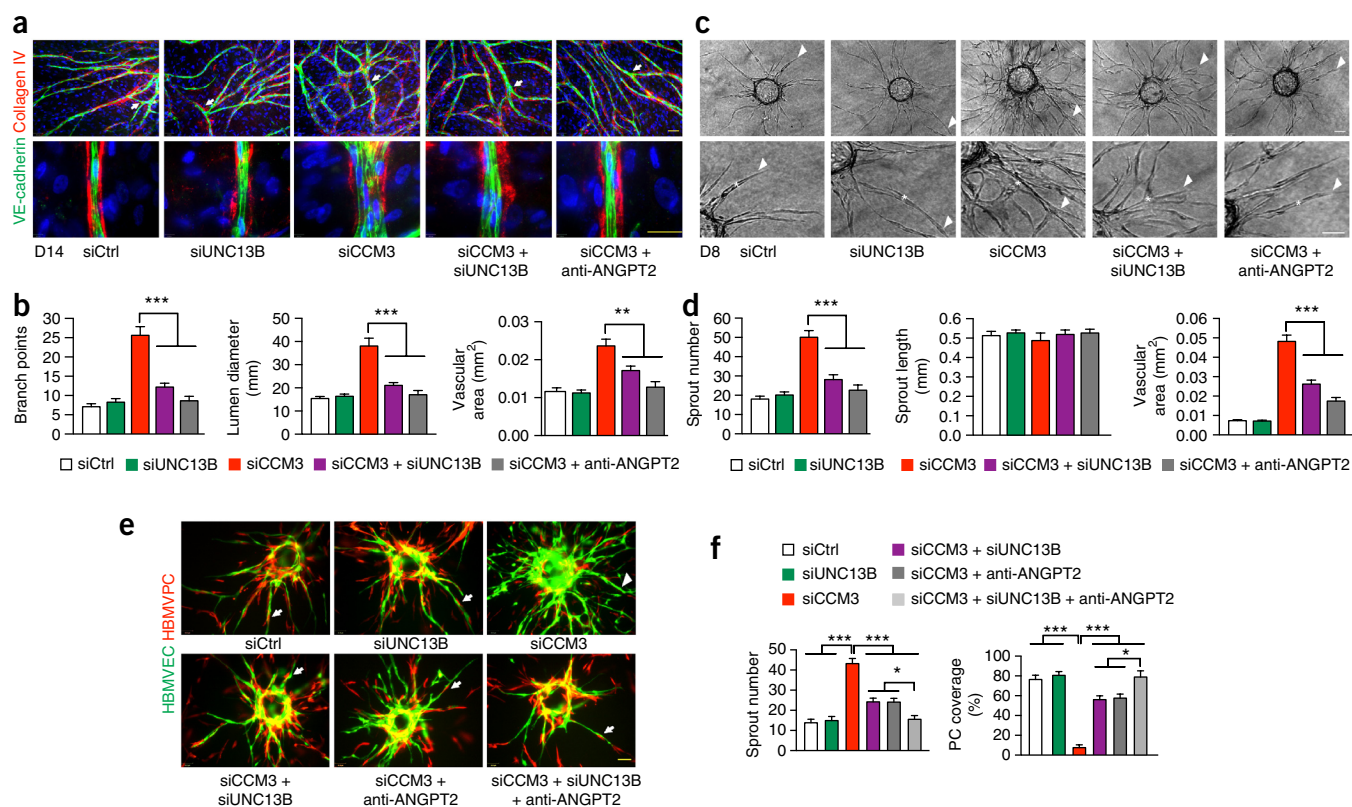
Figure 4 CCM3 maintains normal endothelial lumen formation and endothelial cell–pericyte association. (**a**,**b**) Organotypic angiogenesis assay. 24 h after the transfection of HBMVECs with siRNAs, cells were seeded onto a confluent layer of fibroblasts and were co-cultured for 14 d (D14) in the absence or presence of anti-ANGPT2 (10 μg/ml). Endothelial cell sprouts and lumens were visualized by VE-cadherin and collagen IV staining. Arrows indicate branches. Representative high-power confocal images to visualize the tubule lumen are shown (**a**). Quantification of branch-point numbers, mean lumen diameter and lumen areas (**b**). (**c**,**d**) 3D spheroid sprouting assay. siRNA-transfected HBMVECs were coated with microbeads, embedded in fibrin gels and grown in EGM2 medium for 8 d (D8). A representative image for one of ten beads for each sample is shown; sprouts and lumens are indicated by arrowheads and asterisks, respectively (**c**). Quantification of sprout numbers, sprout length and lumen areas (**d**). (**e**,**f**) Endothelial cell–pericyte interaction in the 3D spheroid sprouting assay. HBMVECs were infected with EGFP-expressing retrovirus, and HBMVPCs were infected with mCherry-expressing lentivirus. Endothelial cells were further transfected with the indicated siRNAs. Endothelial cells and pericytes were seeded in a 2:1 ratio onto beads and treated, as described in **c** and **d**. Endothelial cell sprouts and pericyte coverage were visualized. A representative image for one of ten beads for each sample is shown in **e**; sprouts with or without pericyte coverage are indicated by arrows and arrowheads, respectively. Percentages of pericyte (PC) coverage of sprouts are quantified in **f**. Results shown are representative of at least three separate experiments. $n = 10$ in (**a**–**f**). *$P < 0.05$; **$P < 0.01$; ***$P < 0.001$ (one-way ANOVA). Values are means ± s.e.m. Scale bars, 100 μm.

The knockdown efficiency and specificity of these siRNAs were verified by RT–qPCR (**Supplementary Fig. 4c**). Vesicle fusion events and kinetics were quantified for the individual fusion events recorded in the time-lapse TIRF images. CCM3 silencing in HBMVECs increased the number of exocytic fusion events without affecting the fusion kinetics; moreover, the increased number of fusion events was suppressed by the co-silencing of UNC13B (**Fig. 3c**).

We next examined the direct effect of CCM3 deficiency on ANGPT2 expression and secretion in endothelial cells. WT and CCM3-depleted MBMVECs were isolated[32] and reconstituted by lentiviral transduction with CCM3-WT (1–212 aa) or CCM3-N (1–95 aa) (a loss-of-function CCM3 mutant encoded by a *PDCD10* mutation found in individuals with CCM). ANGPT2 release was increased in CCM3-depleted MBMVECs when compared to WT cells, and this increase was attenuated by reconstitution with CCM3-WT, but not with CCM3-N (**Supplementary Fig. 4d**). In HBMVECs, the silencing of CCM3, but not of CCM1 or CCM2 protein, caused a significant increase in ANGPT2 secretion, and this augmented secretion could be significantly suppressed by co-silencing UNC13B (**Fig. 3d,e**). The levels of *Angpt2* mRNA, however (**Supplementary Fig. 4c**),

and total ANGPT2 protein (**Fig. 3f**) were not significantly altered by the silencing of CCM3 or UNC13B. The increase in ANGPT2 secretion in CCM3-knockdown endothelial cells was associated with enhanced levels of phospho-TIE2. However, total TIE2 and ANGPT1 protein levels were not affected in these cells (**Fig. 3f**). Consistently with previous findings that CCM3 stabilizes GCKIII kinases[33], CCM3 knockdown in HBMVECs induced a reduction in STK24 levels, as compared to those in control cells (**Fig. 3f**).

We next tested the effects of protein synthesis inhibition by cycloheximide (CHX) treatment on ANGPT2 release in HBMVECs. As we reported previously[34], VEGFR2 (encoded by *KDR*) levels were dramatically reduced at 2 h after CHX treatment; by contrast, total ANGPT2, TIE2 and CCM3 protein levels were reduced only at 8 h after CHX treatment (**Supplementary Fig. 4e**), which suggests that these proteins are relatively stable, consistent with previous work showing that CCM3 has a half life of ≥8 h[32]. CHX treatment had no effects on total or secreted ANGPT2 levels in control or CCM3-depleted endothelial cells at 8 h after treatment (**Fig. 3g**). These data are consistent with previous work indicating that ANGPT2 levels are regulated primarily at a step of protein release[28]. We detected
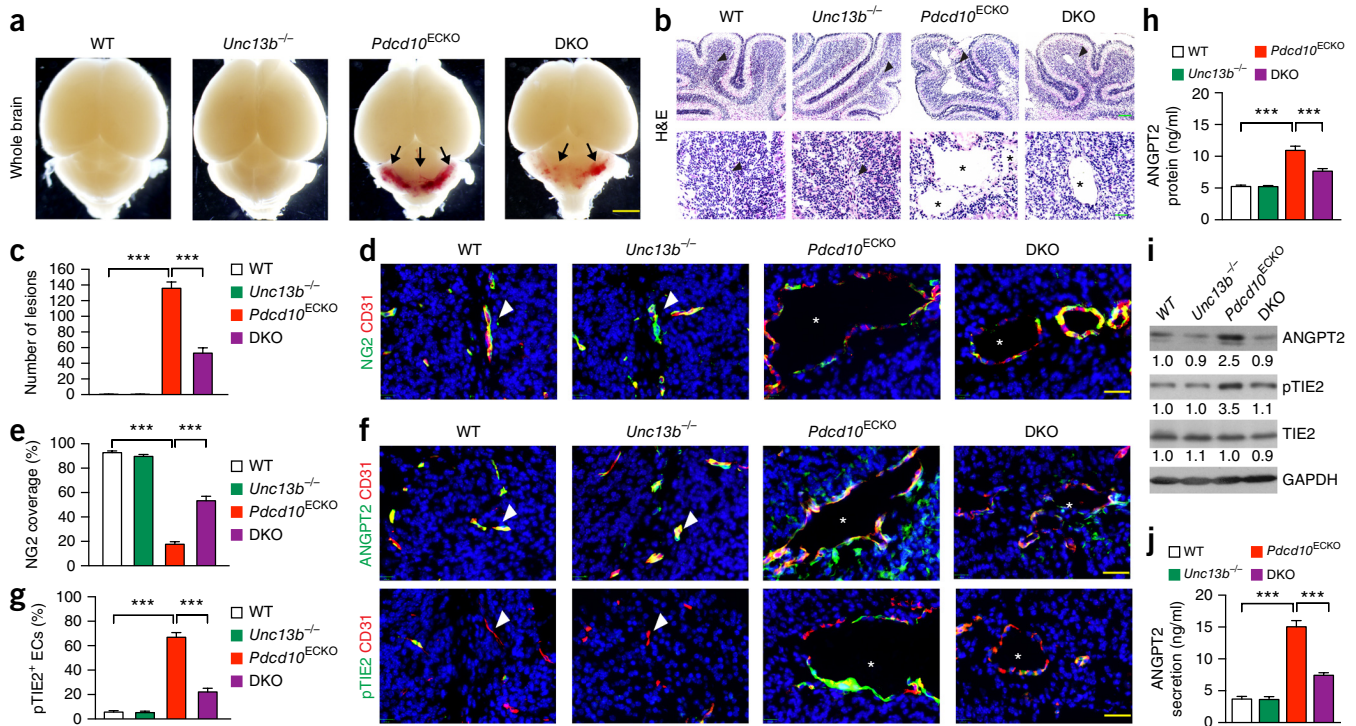
Figure 5 UNC13 deficiency rescues CCM phenotypes in *Pdcd10*[ECKO] mice. (**a**) Images of fresh brain tissue of WT, *Unc13b*^{−/−}, *Pdcd10*[ECKO] and DKO (*Pdcd10*[ECKO];*Unc13b*^{−/−}) pups at P10. Arrows indicate lesions. (**b**) H&E staining of cerebellum sections at P10 and (**c**) quantification of the number of lesions. (**d**,**e**) Co-staining for NG2 with CD31 and quantification of NG2^{+} coverage on microvessels. (**f**,**g**) Co-staining for CD31 with ANGPT2 or pTIE2 (**f**) and quantification of pTIE2-positive endothelial cells (ECs) (**g**). Arrowheads indicate normal vessels and asterisks indicate lesions in images of all panels. Data in **c**,**e**,**g**, are from *n* = 10 mice per group representative of at least three sections per mouse. (**h**,**i**) ANGPT2 levels in brain tissue, as determined by ELISA (**h**) and by western blotting (**i**). *n* = 10 mice per group. (**j**) ANGPT2 levels in culture supernatants of MBMVECs isolated from mice of the indicated genotypes were measured by ELISA; *n* = 10 mice per group. ***$P < 0.001$ (one-way ANOVA). Values are means ± s.e.m. Scale bars, 2 mm (**a**); 400 μm (**b**, top); 100 μm (**b**, bottom; **d**,**f**).

localization of ANGPT2 in VAMP3-positive vesicles in CCM3-knockdown endothelial cells (**Supplementary Fig. 4f**). Enhanced levels of ANGPT2 secretion and phospho-TIE2 in CCM3-depleted endothelial cells were blunted by the co-silencing of VAMP3 (**Supplementary Fig. 4g,h**). We observed a similar role of CCM3 on vWF release and P-selectin surface expression in endothelial cells (**Supplementary Fig. 4i,j**). These data demonstrate that CCM3 restrains exocytosis of ANGPT2 from the WPB in endothelial cells.

Additionally, we examined whether CCM3-mediated ANGPT2 secretion contributes to endothelial-cell-junction and endothelial-barrier integrity. CCM3 knockdown dramatically disrupted both adherens and tight junctions, as detected by immunostaining for VE-cadherin and zonula occludens 1 (ZO1, encoded by *TJP1*), respectively. However, the co-silencing of UNC13B or treatment with anti-ANGPT2 antibody significantly normalized both adherens and tight junctions (**Fig. 3h,i**). Co-silencing of UNC13B or anti-ANGPT2 antibody also restored barrier function in CCM3-ablated endothelial cells, as assessed by transendothelial electric resistance (TEER) using electrical cell-substrate impedance sensing[35] (**Fig. 3j**).

CCM3–ANGPT2 axis regulates endothelial lumen formation and pericyte recruitment

To study how CCM3 regulates vessel lumen diameter, which was observed to be enlarged in the brain tissues of *Pdcd10*[ECKO] mice, we analyzed endothelial cell sprouting and lumen formation using an optimized *in vitro*, endothelial-cell-sprouting and tube-formation

model[36,37]. When EGFP-expressing HBMVECs were seeded onto a confluent layer of fibroblasts, we observed that lumen formation peaked between days 7 and 14 after co-culture (data not shown). CCM3 knockdown resulted in enhanced endothelial cell sprouting and lumen formation, as visualized by VE-cadherin and collagen-IV staining (**Fig. 4a**; **Supplementary Fig. 5a,b**). Quantitative analyses indicated that the number of branch points, mean lumen diameter and lumenized (collagen-IV-covered) area[37,38] was significantly increased in the CCM3-knockdown group, as compared to that in the siCtrl group (**Fig. 4a,b**). The enhancing effects induced by CCM3 knockdown on endothelial cell sprouting and lumen formation were not affected by control IgG treatment, but were blunted by either co-silencing of UNC13B or treatment with anti-ANGPT2 antibody (**Fig. 4a,b**).

To further verify that CCM3 regulates lumen formation and pericyte recruitment, we performed a 3D spheroid sprouting assay in which endothelial cells were coated onto cytodex beads, followed by the embedding of the beads in fibrin gels. Fibroblasts cultured on top of the gel promoted optimal sprouting and tube formation, which peaked at day 8, as visualized by immunostaining with VE-cadherin (**Supplementary Fig. 5c–e**). Quantitative analyses indicated that the mean sprout length was not different between the control and CCM3-knockdown groups, but the number of sprouts was drastically increased by CCM3 knockdown. Moreover, we detected dilated lumen formation in the CCM3-knockdown group (**Supplementary Fig. 5c–f**). Notably, the enhancing effects of CCM3 knockdown on
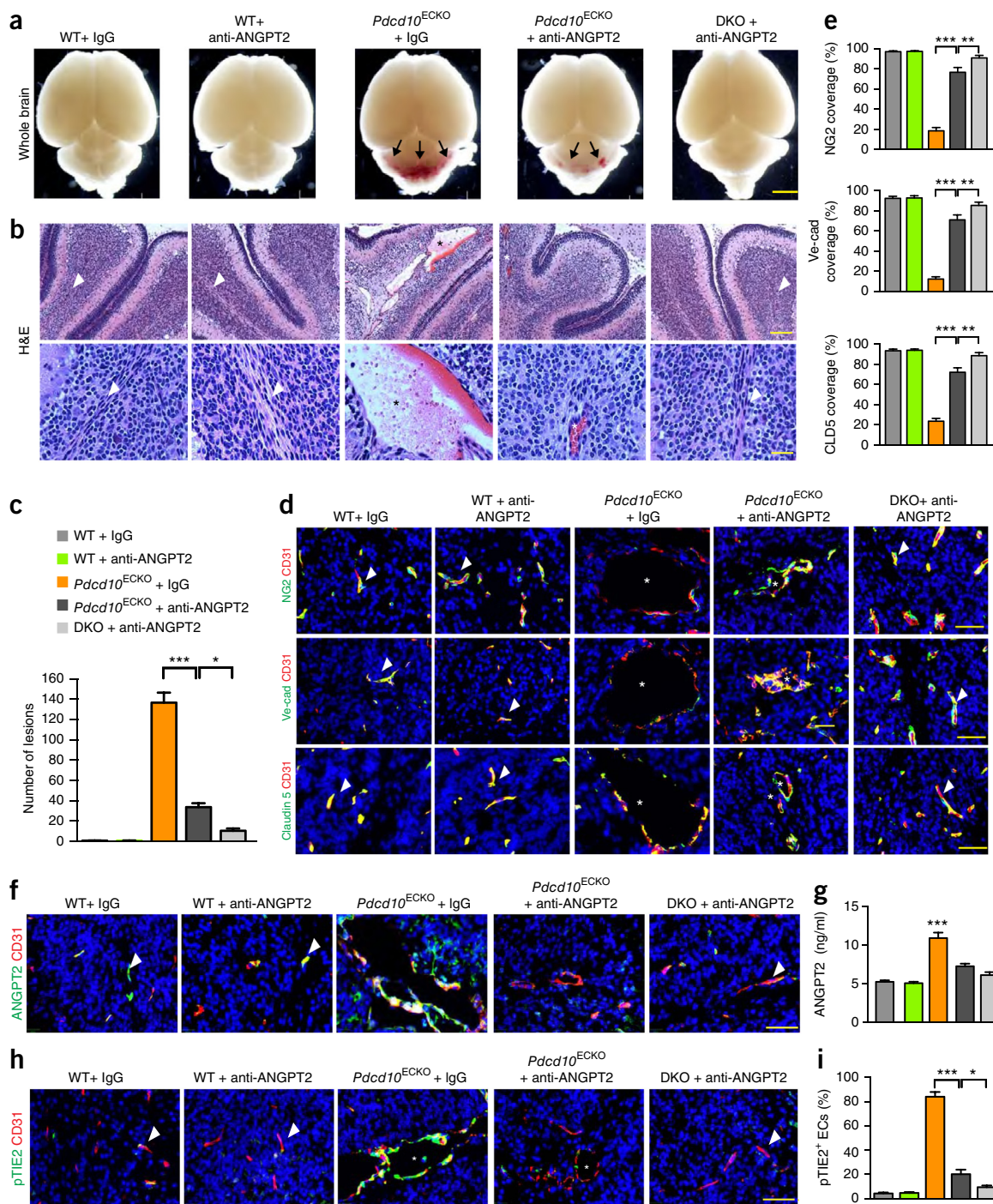
Figure 6 ANGPT2-neutralizing antibody blunts CCM lesion progression in *Pdcd10*ECKO mice. (**a**) Images of fresh brain tissue of WT, *Pdcd10*ECKO and DKO (*Pdcd10*ECKO;*Unc13b*−/−) pups treated with IgG or anti-ANGPT2 antibody. Arrows indicate lesions. (**b,c**) H&E staining of cerebellum sections at P10 and quantification of the number of lesions ($n = 10$ mice per group). (**d,e**) Co-staining of CD31 with NG2, VE-cadherin or claudin 5 (**d**); and quantification of NG2, VE-cadherin and claudin 5 coverage on microvessels (**e**) ($n = 10$ mice per group). (**f**) Co-staining of ANGPT2 with CD31. (**g**) ANGPT2 levels in brain tissue were determined by ELISA ($n = 10$ mice per group). (**h,i**) Co-staining for pTIE2 with CD31 (**h**) and quantification of pTIE2-positive endothelial cells (**i**). Arrowheads indicate normal or normalized vessels, and asterisks indicate lesions in **b,d,f** and **h**. *$P < 0.05$, **$P < 0.01$, ***$P < 0.001$ (one-way ANOVA). Values are means ± s.e.m. Scale bars, 2 mm (**a**); 400 μm (**b**, top); 100 μm (**b**, bottom; **d,f,h**).

endothelial cell sprouting and lumen formation in this assay were blunted by either co-silencing of UNC13B or treatment with anti-ANGPT2 antibody (**Fig. 4c,d**).

The spheroid sprouting assay has been used as a system to study pericyte or smooth-muscle cell recruitment and vessel maturation[39].

To visualize endothelial cells and pericytes in the sprouts, EGFP-expressing HBMVECs were transfected with a control or CCM3 siRNA and then seeded with mCherry-expressing normal human brain microvascular pericytes (HBMVPCs). Pericytes were recruited to control endothelial cells, but not to CCM3-knockdown endothelial

cells, during sprouting (**Fig. 4e**). However, co-silencing of UNC13B in the endothelial cells or treatment with anti-ANGPT2 antibody, or a combination of both, restored pericyte recruitment to endothelial cell sprouts (**Fig. 4e,f**). These data suggest that CCM3 maintains normal endothelial cell junctions, endothelial cell lumen formation and pericyte recruitment by restraining ANGPT2 exocytosis from endothelial cells.

Unc13b deficiency reduces ANGPT2 secretion and CCM lesions in *Pdcd10*[ECKO] mice

Unc13b^{−/−} mice do not show gross phenotypes, but they develop seizures after 1 year of age, probably owing to a requirement for UNC13 function in the brain[40]. To test whether the suppression of elevated exocytosis rescues CCM-associated defects in CCM3-deficient mice, *Pdcd10*[ECKO];*Unc13b*^{−/−} (double knockout, DKO) mice were obtained by mating *Unc13b*^{−/−} mice with *Cdh5-CreERT2*;*Pdcd10*^{fl/fl} mice, followed by feeding pups with tamoxifen at P1–P3. Brain tissue was harvested at P5 (early in lesion development) and P10 (full lesion development). No lesions were found in the brain of *Unc13b*^{−/−} mice (**Fig. 5a–c**). The numbers of lesions (**Fig. 5a–c**) and enlarged vessels with defects in pericyte coverage in cerebellar sections (**Fig. 5d,e**) were significantly reduced in DKO mice, as compared to those in *Pdcd10*[ECKO] mice. Diffuse ANGPT2 staining surrounding dilated vessels and a concomitant increase in phospho-TIE2 staining of endothelial cells were detected in *Pdcd10*[ECKO] mice, as compared to WT or *Unc13b*^{−/−} mice, and these effects were normalized in DKO mice (**Fig. 5f,g**). Total ANGPT2 protein levels in brain tissue were weakly upregulated by CCM3 deficiency, and this effect was normalized by *Unc13b* deletion, as measured by ELISA and western blotting (**Fig. 5h,i**). Similarly, ANGPT2 secretion was increased significantly in brain endothelial cells isolated from the diseased brain of *Pdcd10*[ECKO] mice, and this effect was also normalized by co-deletion of *Unc13b* (**Fig. 5j**). These results strongly suggest that UNC13B deficiency, by suppressing ANGPT2–TIE2 signaling in endothelial cells, attenuates the neurovascular phenotype caused by *Pdcd10* inactivation.

ANGPT2-neutralizing antibody blocks CCM lesion formation in *Pdcd10*[ECKO] mice

Anti-ANGPT2 antibody strongly inhibits angiogenesis at high doses[38,41]. When administered by intraperitoneal (i.p.) injection at 10 μg/g (body weight) from P2 and every other day thereafter, we observed modest inhibitory effects of anti-ANGPT2 on retinal angiogenesis (~22%) and brain vascular density (~10%) (**Supplementary Fig. 6**). By contrast, ANGPT2 neutralization dramatically reduced the number of CCM lesions in *Pdcd10*[ECKO] mice, as compared to untreated mice, as visualized by whole-mount and H&E staining (**Fig. 6a–c**). We further tested the combinatory effects of ANGPT2 antibody treatment and *Unc13b* deficiency on CCM lesion development. ANGPT2-antibody administration to DKO mice completely abrogated CCM lesion formation in the brain (**Fig. 6a–c**) and in the retina (**Supplementary Fig. 7a–c**). Chondroitin sulfate proteoglycan 4 (CSPG4, also known as NG2)-positive pericyte coverage of CD31^{+} microvessels was enhanced by ANGPT2-antibody treatment, from 20% in IgG-treated *Pdcd10*[ECKO] mice to more than 80% in ANGPT2-antibody-treated *Pdcd10*[ECKO] mice, and pericyte coverage was almost 100% in ANGPT2-antibody-treated DKO mice (**Fig. 6d,e**). We observed similar results for endothelial cell adherens and tight junctions (**Fig. 6d,e**). Next, we determined whether the therapeutic effects of ANGPT2 antibody were associated with effects on ANGPT2–TIE2 signaling *in vivo*. Diffuse ANGPT2 staining surrounding dilated vessels, increased phospho-TIE2 staining in endothelial cells and an increase in total ANGPT2 protein were all observed in *Pdcd10*[ECKO] mice, as compared to WT mice; these defects were normalized by ANGPT2-antibody treatment of *Pdcd10*[ECKO] and abolished by ANGPT2-antibody treatment of DKO mice (**Fig. 6f–i**). Taken together, these data support the conclusion that CCM3 deficiency induces ANGPT2 secretion from endothelial cells, which disrupts endothelial cell junctions and endothelial cell–pericyte association and contributes to the CCM disease phenotype.

DISCUSSION

In this study, we report that CCM lesions in mice with an endothelial-cell-specific *Pdcd10* gene deletion (*Pdcdc10*[ECKO]) exhibit cerebellar hemorrhage with disrupted endothelial cell junctions and endothelial cell–pericyte associations, which is correlated with increased ANGPT2 secretion surrounding dilated cerebral microvessels. This enhanced ANGPT2 secretion was observed in brain and retinal tissue, but not in lung tissue or blood. This type of brain- and retina-specific effect of CCM3 on ANGPT2 secretion provides a possible explanation for the restriction of CCM lesions to the brain and retina of endothelial-cell-specific, CCM3-deficient mice. Studies *in vitro* confirmed that CCM3 deficiency in endothelial cells causes a disruption of endothelial-cell junctions, enlarged lumen formation and reduced pericyte recruitment during sprouting and tube formation, as compared to WT cells. These endothelial-cell phenotypes are associated with augmented ANGPT2 release and secretion, and they are substantially attenuated by the inhibition of exocytosis or neutralization of ANGPT2, which suggests that CCM3 maintains normal endothelial cell junctions, lumen formation and vessel maturation by restraining exocytosis-mediated ANGPT2 release from endothelial cells. Mechanistic studies using confocal and TIRF microscopy analyses suggested that CCM3, by suppressing UNC13B- and VAMP-dependent exocytosis, regulates ANGPT2 release from WPBs in brain endothelial cells. Using mouse genetic approaches, we showed that *Unc13b*-deficiency prevents the disruption of endothelial-cell junctions and vessel dilation and blocks CCM lesion development in the brain of endothelial-cell-specific, CCM3-deficient mice. Notably, an ANGPT2-neutralizing antibody ameliorates CCM lesion progression in the mouse CCM model, which is associated with normalization of endothelial cell junctions, endothelial cell–pericyte interaction and vascular integrity. Our study reveals a new mechanism by which *PDCD10* mutation contributes to the progression of the CCM disease (**Supplementary Fig. 8**), and thus offers a potential therapeutic approach to this presently incurable pathology.

We recently demonstrated that CCM3, in a complex with GCKIII kinases, binds to the C2B domain of UNC13 and inhibits its binding to plasma membrane lipids—a step required for exocytosis[24]. In the present study, we provide strong evidence that CCM3, through its effects on UNC13B- and VAMP-dependent exocytosis, controls ANGPT2 secretion in endothelial cells. We found that UNC13B is the primary isoform expressed in vascular endothelial cells, and that UNC13B forms a complex with CCM3 and the GCKIII member STK24 in endothelial cells. By confocal microscopy, we showed that CCM3 co-localizes with VAMP3 and VAMP8 in brain endothelial cells, and by real-time TIRF microscopic analyses, that CCM3 depletion increases exocytic fusion events, which can be suppressed by co-silencing UNC13B. Depletion of CCM3 (but not of CCM1 or CCM2) in brain endothelial cells strongly augments ANGPT2 secretion from the cells, which could be blocked by co-silencing of UNC13B or VAMP3. However, *Angpt2* mRNA and total ANGPT2 protein are not dramatically altered by CCM3

deletion in endothelial cells, and ANGPT2 protein stability and secretion are not altered in CCM3-depleted endothelial cells, which supports the concept that the primary mechanism for the increase in ANGPT2 release resulting from CCM3 deficiency is exocytosis rather than effects on protein synthesis or stability. Using genetic approaches involving *Pdcd10*- and *Unc13b*-deficient mice, we observed similar regulatory patterns of ANGPT2 secretion by CCM3 and UNC13B in mouse brain and retinal tissue.

Although *Angpt2*-deficient mice are viable[42], ANGPT2 is required for postnatal angiogenesis and lymphatic patterning[42]. Defects in ANGPT2 function might cause glaucoma, a disease that leads to blindness[43]. For clinical translation of the finding that treatment with a ANGPT2-neutralizing antibody attenuates CCM lesions in CCM3-deficient mice, it might be necessary to optimize the dose of the antibody to achieve a maximal anti-CCM effect, with minimal side effects on physiological vascular development and function.

The TIE2-signaling pathway has distinct roles in both vascular quiescence and angiogenesis. These effects have been attributed to distinct TIE2-signaling complexes assembled by ANGPT1, such that phospho-TIE2 is located at endothelial cell–endothelial cell contacts in the quiescent state, but at endothelial cell–matrix contacts during angiogenesis[44,45]. Although ANGPT2 acts as a negative regulator of ANGPT1–TIE2 signaling in quiescent endothelial cells, it is capable of inducing TIE2 phosphorylation in stressed endothelial cells[38,46]. We observed increased ANGPT2–TIE2 signaling in CCM3-depleted endothelial cells, consistent with a report that *PDCD10* deletion induces several forms of stress-related signaling in endothelial cells[47]. Our data indicate that increased ANGPT2 secretion in both CCM3-depleted brain tissues and brain endothelial cells correlates with enhanced phospho-TIE2 levels. It is plausible that ANGPT2 antagonizes ANGPT1 in quiescent endothelial cells to inhibit TIE2 activation, whereas it synergizes with ANGPT1 in inducing TIE2 phosphorylation to promote angiogenesis, and our data clearly demonstrate that enhanced ANGPT2–TIE2 signaling contributes to CCM pathogenesis. The pathological consequences of increased ANGPT2–TIE2 signaling resulting from CCM3 loss might, however, be different from the consequences of the acute ANGPT2–TIE2 activation that occurs during acute inflammation such as sepsis[48]; CCM3 loss, but not sepsis, has strong effects on increasing endothelial lumen dilatation. Loss of CCM1 or CCM2 in endothelial cells activates several signaling pathways, including RhoA[49], MEKK3–ERK5–Krüppel-like factor (KLF) 2/4 signaling[20,50] and KLF4–TGF-β–Smad-mediated endothelial-mesenchymal transition (EndMT)[16,50]. It needs to be further defined whether the CCM3–UNC13–ANGPT2–TIE2 axis participates in cross-talk with these pathways. Notably, ANGPT1–TIE2, acting via PI3K–Akt activation, induces the expression of KLF2 in quiescent endothelial cells[51]. It is possible that in CCM3-depleted endothelial cells, ANGPT2, acting via TIE2, induces KLF2 protein expression, which serves as a point of convergence for CCM3-mediated, ANGPT2–TIE2 signaling and CCM1/2-mediated MEKK3–ERK5 signaling.

The modulation of endothelial cell junctions is emerging as a common mechanism by which defects in signaling pathways resulting from mutations (in humans) or deletions (in postnatal mice) in any of the three CCM genes result in similar CCM lesions. CCM1, in a complex with CCM2, binds to and regulates several proteins that are directly involved in endothelial cell junctions and junction-associated complexes, such as RAP1, heart-development protein with EGF-like domains 1 (HEG1) and integrin cytoplasmic domain–associated protein 1 (ICAP1, encoded by *ITGB1BP1*)[52–54]. Our data from studies both *in vitro* and *in vivo* demonstrate that CCM3, by restraining

ANGPT2 secretion, regulates both adherens and tight junctions in brain endothelial cells. It remains unknown exactly how alterations of endothelial cell junctions are linked to CCM lesion development. A common phenotype of CCM gene deletions is enlarged lumen formation, and it is known that endothelial-cell-junction organization directly regulates endothelial lumen formation[55]. In the early mouse embryo, a homozygous null mutation of the gene encoding VE-cadherin (*Cdh5*) results in enlarged lumens of cephalic vessels, although the lumenal sizes of the aorta and cardinal veins are reduced, as compared to those in WT mice[56,57]. Mechanistic studies suggest that CCM1–VE-cadherin affects the association of the adherens junction with the polarity complex to regulate vascular lumenal structure[55], and that CCM3 might have similar effects. Alternatively, CCM3-mediated exocytosis might directly contribute to lumen formation. It is now accepted that lumen formation involves the structured expansion of the apical plasma membrane through the general mechanism of vesicle transport[58]. This idea is supported by recent reports from genetic studies of tracheal tubule formation in *Drosophila*. Mutant flies with loss-of-function mutations in the genes encoding orthologs of CCM3 or GCKIII kinase have dilated tracheal tubes, which resemble the dilated blood vessels found in people with CCM[59]. This tube-dilation phenotype can be suppressed by a reduction in the expression of NSF2, a protein involved in SNARE recycling and the secondary phase of exocytosis. Moreover, CCM lesions are found predominantly in vessels of the brain and retina, which are notable for having an extraordinarily high pericyte-to-endothelial-cell ratio, thereby forming a high-resistance blood–brain barrier or blood–retinal barrier, which is further supplemented by astrocyte foot processes. Our *in vitro* model study indicated that a loss of CCM3 in endothelial cells causes dilated lumen with impaired pericyte recruitment, recapitulating the CCM lesion phenotype *in vivo*, and thus indicates that ANGPT2 has a crucial role in the modulation of CCM3-mediated endothelial cell–pericyte interactions. The identification of ANGPT2 as a CCM3 (but not CCM1 or CCM2)-downstream effector might explain why *PDCD10* mutations in humans often result in a more severe form of the disease, as compared to mutations in *KRIT1* or *CCM2*.

METHODS

Methods and any associated references are available in the online version of the paper.

Note: Any Supplementary Information and Source Data files are available in the online version of the paper.

AUTHOR CONTRIBUTIONS

H.J.Z., L.Q., H.Z. and W.M. conceived the study, designed experiments and wrote the manuscript; H.J.Z., L.Q., H.Z., W.T., W.J., Y.H., Z.W., Q.Y. and M.S.K. performed experiments; W.J., G.F. and M.Y. generated the anti-angiopoietin-2 antibodies; X.L. interpreted retinal data; A.V. provided the human CCM blocks; and H.J.Z., L.Q., H.Z., D.T., D.W. and W.M. interpreted data. M.S.K. edited the manuscript.

COMPETING FINANCIAL INTERESTS

The authors declare competing financial interests: details are available in the online version of the paper.

ARTICLES

Reprints and permissions information is available online at http://www.nature.com/reprints/index.html.

1. Revencu, N. & Vikkula, M. Cerebral cavernous malformation: new molecular and clinical insights. *J. Med. Genet.* **43**, 716–721 (2006).
2. Cavalcanti, D.D. *et al.* Cerebral cavernous malformations: from genes to proteins to disease. *J. Neurosurg.* **116**, 122–132 (2012).
3. Tanriover, G. *et al.* Ultrastructural analysis of vascular features in cerebral cavernous malformations. *Clin. Neurol. Neurosurg.* **115**, 438–444 (2013).
4. Riant, F., Bergametti, F., Ayrignac, X., Boulday, G. & Tournier-Lasserve, E. Recent insights into cerebral cavernous malformations: the molecular genetics of CCM. *FEBS J.* **277**, 1070–1075 (2010).
5. Labauge, P., Denier, C., Bergametti, F. & Tournier-Lasserve, E. Genetics of cavernous angiomas. *Lancet Neurol.* **6**, 237–244 (2007).
6. Sahoo, T. *et al.* Mutations in the gene encoding KRIT1, a Krev-1/rap1a binding protein, cause cerebral cavernous malformations (CCM1). *Hum. Mol. Genet.* **8**, 2325–2333 (1999).
7. Liquori, C.L. *et al.* Mutations in a gene encoding a novel protein containing a phosphotyrosine-binding domain cause type 2 cerebral cavernous malformations. *Am. J. Hum. Genet.* **73**, 1459–1464 (2003).
8. Bergametti, F. *et al.* Mutations within the programmed cell death 10 gene cause cerebral cavernous malformations. *Am. J. Hum. Genet.* **76**, 42–51 (2005).
9. Gault, J., Shenkar, R., Recksiek, P. & Awad, I.A. Biallelic somatic and germ line CCM1 truncating mutations in a cerebral cavernous malformation lesion. *Stroke* **36**, 872–874 (2005).
10. Akers, A.L., Johnson, E., Steinberg, G.K., Zabramski, J.M. & Marchuk, D.A. Biallelic somatic and germline mutations in cerebral cavernous malformations (CCMs): evidence for a two-hit mechanism of CCM pathogenesis. *Hum. Mol. Genet.* **18**, 919–930 (2009).
11. Pagenstecher, A., Stahl, S., Sure, U. & Felbor, U. A two-hit mechanism causes cerebral cavernous malformations: complete inactivation of CCM1, CCM2 or CCM3 in affected endothelial cells. *Hum. Mol. Genet.* **18**, 911–918 (2009).
12. McDonald, D.A. *et al.* A novel mouse model of cerebral cavernous malformations based on the two-hit-mutation hypothesis recapitulates the human disease. *Hum. Mol. Genet.* **20**, 211–222 (2011).
13. Chan, A.C. *et al.* Mutations in 2 distinct genetic pathways result in cerebral cavernous malformations in mice. *J. Clin. Invest.* **121**, 1871–1881 (2011).
14. Cunningham, K. *et al.* Conditional deletion of Ccm2 causes hemorrhage in the adult brain: a mouse model of human cerebral cavernous malformations. *Hum. Mol. Genet.* **20**, 3198–3206 (2011).
15. Boulday, G. *et al.* Tissue-specific conditional CCM2 knockout mice establish the essential role of endothelial CCM2 in angiogenesis: implications for human cerebral cavernous malformations. *Dis. Model. Mech.* **2**, 168–177 (2009).
16. Maddaluno, L. *et al.* EndMT contributes to the onset and progression of cerebral cavernous malformations. *Nature* **498**, 492–496 (2013).
17. Shenkar, R. *et al.* Exceptional aggressiveness of cerebral cavernous malformation disease associated with *PDCD10* mutations. *Genet. Med.* **17**, 188–196 (2015).
18. Whitehead, K.J. *et al.* The cerebral cavernous malformation signaling pathway promotes vascular integrity via Rho GTPases. *Nat. Med.* **15**, 177–184 (2009).
19. Stockton, R.A., Shenkar, R., Awad, I.A. & Ginsberg, M.H. Cerebral cavernous malformations proteins inhibit Rho kinase to stabilize vascular integrity. *J. Exp. Med.* **207**, 881–896 (2010).
20. Zhou, Z. *et al.* Cerebral cavernous malformations arise from endothelial gain of MEKK3–KLF2/4 signalling. *Nature* **532**, 122–126 (2016).
21. Denier, C. *et al.* Genotype-phenotype correlations in cerebral cavernous malformations patients. *Ann. Neurol.* **60**, 550–556 (2006).
22. Zheng, X. *et al.* CCM3 signaling through sterile 20-like kinases plays an essential role during zebrafish cardiovascular development and cerebral cavernous malformations. *J. Clin. Invest.* **120**, 2795–2804 (2010).
23. Yoruk, B., Gillers, B.S., Chi, N.C. & Scott, I.C. Ccm3 functions in a manner distinct from Ccm1 and Ccm2 in a zebrafish model of CCM vascular disease. *Dev. Biol.* **362**, 121–131 (2012).
24. Zhang, Y. *et al.* A network of interactions enables CCM3 and STK24 to coordinate UNC13D-driven vesicle exocytosis in neutrophils. *Dev. Cell* **27**, 215–226 (2013).
25. Feldmann, J. *et al.* Munc13-4 is essential for cytolytic granules fusion and is mutated in a form of familial hemophagocytic lymphohistiocytosis (FHL3). *Cell* **115**, 461–473 (2003).
26. Jahn, R. & Südhof, T.C. Membrane fusion and exocytosis. *Annu. Rev. Biochem.* **68**, 863–911 (1999).
27. Lowenstein, C.J., Morrell, C.N. & Yamakuchi, M. Regulation of Weibel-Palade body exocytosis. *Trends Cardiovasc. Med.* **15**, 302–308 (2005).
28. Fiedler, U. *et al.* Angiopoietin-2 sensitizes endothelial cells to TNF-α and has a crucial role in the induction of inflammation. *Nat. Med.* **12**, 235–239 (2006).
29. Gaengel, K., Genové, G., Armulik, A. & Betsholtz, C. Endothelial-mural cell signaling in vascular development and angiogenesis. *Arterioscler. Thromb. Vasc. Biol.* **29**, 630–638 (2009).
30. Eklund, L. & Olsen, B.R. Tie receptors and their angiopoietin ligands are context-dependent regulators of vascular remodeling. *Exp. Cell Res.* **312**, 630–641 (2006).
31. Maisonpierre, P.C. *et al.* Angiopoietin-2, a natural antagonist for Tie2 that disrupts *in vivo* angiogenesis. *Science* **277**, 55–60 (1997).
32. He, Y. *et al.* Stabilization of VEGFR2 signaling by cerebral cavernous malformation 3 is critical for vascular development. *Sci. Signal.* **3**, ra26 (2010).
33. Fidalgo, M. *et al.* CCM3/PDCD10 stabilizes GCKIII proteins to promote Golgi assembly and cell orientation. *J. Cell Sci.* **123**, 1274–1284 (2010).
34. Zhou, H.J. *et al.* AIP1 mediates vascular endothelial cell growth factor receptor-3-dependent angiogenic and lymphangiogenic responses. *Arterioscler. Thromb. Vasc. Biol.* **34**, 603–615 (2014).
35. Kluger, M.S., Clark, P.R., Tellides, G., Gerke, V. & Pober, J.S. Claudin-5 controls intercellular barriers of human dermal microvascular but not human umbilical vein endothelial cells. *Arterioscler. Thromb. Vasc. Biol.* **33**, 489–500 (2013).
36. Nakatsu, M.N. & Hughes, C.C. An optimized three-dimensional in vitro model for the analysis of angiogenesis. *Methods Enzymol.* **443**, 65–82 (2008).
37. Abraham, S. *et al.* A Rac/Cdc42 exchange factor complex promotes formation of lateral filopodia and blood vessel lumen morphogenesis. *Nat. Commun.* **6**, 7286 (2015).
38. Felcht, M. *et al.* Angiopoietin-2 differentially regulates angiogenesis through TIE2 and integrin signaling. *J. Clin. Invest.* **122**, 1991–2005 (2012).
39. Chang, W.G., Andrejecsk, J.W., Kluger, M.S., Saltzman, W.M. & Pober, J.S. Pericytes modulate endothelial sprouting. *Cardiovasc. Res.* **100**, 492–500 (2013).
40. Varoqueaux, F. *et al.* Total arrest of spontaneous and evoked synaptic transmission but normal synaptogenesis in the absence of Munc13-mediated vesicle priming. *Proc. Natl. Acad. Sci. USA* **99**, 9037–9042 (2002).
41. Holopainen, T. *et al.* Effects of angiopoietin-2-blocking antibody on endothelial cell-cell junctions and lung metastasis. *J. Natl. Cancer Inst.* **104**, 461–475 (2012).
42. Gale, N.W. *et al.* Angiopoietin-2 is required for postnatal angiogenesis and lymphatic patterning, and only the latter role is rescued by Angiopoietin-1. *Dev. Cell* **3**, 411–423 (2002).
43. Thomson, B.R. *et al.* A lymphatic defect causes ocular hypertension and glaucoma in mice. *J. Clin. Invest.* **124**, 4320–4324 (2014).
44. Saharinen, P. *et al.* Angiopoietins assemble distinct Tie2 signalling complexes in endothelial cell-cell and cell-matrix contacts. *Nat. Cell Biol.* **10**, 527–537 (2008).
45. Fukuhara, S. *et al.* Differential function of Tie2 at cell-cell contacts and cell-substratum contacts regulated by angiopoietin-1. *Nat. Cell Biol.* **10**, 513–526 (2008).
46. Daly, C. *et al.* Angiopoietin-2 functions as an autocrine protective factor in stressed endothelial cells. *Proc. Natl. Acad. Sci. USA* **103**, 15491–15496 (2006).
47. Marchi, S. *et al.* Defective autophagy is a key feature of cerebral cavernous malformations. *EMBO Mol. Med.* **7**, 1403–1417 (2015).
48. Kümpers, P. *et al.* Time course of angiopoietin-2 release during experimental human endotoxemia and sepsis. *Crit. Care* **13**, R64 (2009).
49. Gingras, A.R., Liu, J.J. & Ginsberg, M.H. Structural basis of the junctional anchorage of the cerebral cavernous malformations complex. *J. Cell Biol.* **199**, 39–48 (2012).
50. Cuttano, R. *et al.* KLF4 is a key determinant in the development and progression of cerebral cavernous malformations. *EMBO Mol. Med.* **8**, 6–24 (2015).
51. Sako, K. *et al.* Angiopoietin-1 induces Kruppel-like factor 2 expression through a phosphoinositide 3-kinase/AKT-dependent activation of myocyte enhancer factor 2. *J. Biol. Chem.* **284**, 5592–5601 (2009).
52. Zawistowski, J.S. *et al.* CCM1 and CCM2 protein interactions in cell signaling: implications for cerebral cavernous malformations pathogenesis. *Hum. Mol. Genet.* **14**, 2521–2531 (2005).
53. Pouwels, J., Nevo, J., Pellinen, T., Ylänne, J. & Ivaska, J. Negative regulators of integrin activity. *J. Cell Sci.* **125**, 3271–3280 (2012).
54. Brütsch, R. *et al.* Integrin cytoplasmic domain-associated protein-1 attenuates sprouting angiogenesis. *Circ. Res.* **107**, 592–601 (2010).
55. Lampugnani, M.G. *et al.* CCM1 regulates vascular-lumen organization by inducing endothelial polarity. *J. Cell Sci.* **123**, 1073–1080 (2010).
56. Carmeliet, P. *et al.* Targeted deficiency or cytosolic truncation of the VE-cadherin gene in mice impairs VEGF-mediated endothelial survival and angiogenesis. *Cell* **98**, 147–157 (1999).
57. Gory-Fauré, S. *et al.* Role of vascular endothelial-cadherin in vascular morphogenesis. *Development* **126**, 2093–2102 (1999).
58. Sigurbjörnsdóttir, S., Mathew, R. & Leptin, M. Molecular mechanisms of de novo lumen formation. *Nat. Rev. Mol. Cell Biol.* **15**, 665–676 (2014).
59. Song, Y., Eng, M. & Ghabrial, A.S. Focal defects in single-celled tubes mutant for cerebral cavernous malformation 3, GCKIII, or NSF2. *Dev. Cell* **25**, 507–519 (2013).

ONLINE METHODS

Generation of tamoxifen-inducible, endothelial-specific CCM3-deficient mice (*Pdcd10*ECKO). *mT/mG*-reporter mice were purchased from The Jackson Laboratory (stock no. 007576; strain name STOCK Gt *(ROSA)26Sor*tm4(ACTB-tdTomato,-EGFP)Luo/J). *Pdcd10*fl/fl mice were crossed with *Cdh5-CreERT2* mice in which the Cre-recombinase expression is driven by the *Cdh*5 promoter to generate mice with inducible endothelial-cell-specific deletion of *Pdcd10* (designated *Pdcd10*ECKO). For tamoxifen-induced *Pdcd10* deletion *in vivo*, tamoxifen (Sigma-Aldrich, T5648) was diluted at 10 mg/ml and fed 10 µg/g (body weight) once daily from P1 to P3 to *Pdcd10*ECKO and WT control mice (*Pdcd10*fl/fl) newborn pups. *Unc13b*-deficient mice[40] do not show gross phenotypes but develop seizures after 1 year of age, probably resulting from the loss of UNC13 function in the brain[40]. For quantification of the number and size of *Pdcd10*ECKO lesions at P5 and P10, serial sagittal frozen or paraffin sections (50 µm) from brain of *Pdcd10*ECKO, *Unc13b*−/− or DKO mice, in some cases treated with IgG1 or anti-ANGPT2 antibody, were obtained. Each section was stained with H&E. Analysis of the number and size of the CCM caverns was performed using an Olympus BX51 microscope and NIS Element imaging software (Nikon). Two different groups of caverns were defined according to their size (< and >10,000 µm²). Mice were cared for in accordance with US National Institutes of Health guidelines, and all procedures were approved by the Yale University Animal Care and Use Committee.

Clinical specimens. Ethical evaluation for the clinical specimens was reviewed and approved by the Yale Human Investigation Committee (IHC# 0601000969). The Section of Neuropathology, Department of Pathology at the Yale University School of Medicine archives human specimens, including cerebral sections, from individuals with *PDCD10* mutations from patients or family members giving informed consent. All of the samples were evaluated independently by two pathologists, who are experienced in evaluating immunohistochemistry and had no prior information regarding the clinical outcome of the patients. We obtained paraffin blocks for eight cases of cerebral sections from individuals with *PDCD10* mutations and serial 5-µm-thick sections (~20) were cut from each block for H&E staining and immunostaining. According to H&E staining, we found that six samples contained typical CCM lesions with normal surrounding tissues, two cases showed severe vascular fibrosis (**Supplementary Fig. 3**).

Treatment with ANGPT2-neutralizing antibody *in vivo*. Humanized mouse monoclonal ANGPT2-neutralizing antibody (Genentech or Darron Medscience) was dissolved in sterile PBS at 1 mg/ml. ANGPT2-neutralizing antibody or control IgG1 was i.p. injected (10 µg/g body weight) to WT (*Pdcd10*fl/fl) and *Pdcd10*ECKO littermates from P2 and every other day thereafter.

FITC-dextran perfusion and Evans blue-dye (EBD) permeability assays. FITC-dextran (FD2000S; Sigma-Aldrich, St. Louis, MO, USA) was dissolved in sterile normal saline at a concentration of 50 mg/ml followed by centrifugation at 10,000*g* for 5 min. The supernatant was collected and protected from light and then injected. WT and *Pdcd10*ECKO littermates with or without anti-ANGPT2 treatment were weighed and anesthetized with an i.p. injection of anesthetic (ketamine) (100 mg/kg) + xylazine 10 mg/kg). The retro-orbital injection followed published protocols[60]. Briefly, the lateral canthus of the left orbit was chosen as the injection site. A 31-gauge needle with a 3/10-ml insulin syringe was used to gently pierce into the mouse's orbital venous sinus, with about 2–3 mm with the bevel of the needle facing upward at a 45° angle. 10 µl per g body weight of FITC-dextran was injected into each pup. After 5 min, brains and retinas were harvested and fixed for sectional or whole-mount fluorescence immunostaining.

For the EBD permeability assay (Miles assay), Evans blue dye (100 µl of a 1% solution in 0.9% NaCl; Sigma-Aldrich) was injected into the retro-orbital plexus of anesthetized WT and *Pdcd10*ECKO mice. 30 min after the injection, mice were euthanized and perfused with PBS through the left ventricle to clear the dye from the vascular volume. Cerebellum tissue was harvested and dried at 60 °C overnight, and weighed before Evans blue extraction using 1 ml of formamide at 55 °C for 16 h. Evans blue content was quantified by reading absorbance at 630 nm in a spectrophotometer.

Immunofluorescence analysis. Mouse brains were harvested, fixed with 4% PFA, embedded in OCT and sectioned (5-µm thick). Slides were washed with PBS twice to remove OCT, and 5% donkey serum in 0.3% TritonX-100 in PBS was used for 30 min to block nonspecific staining and to permeabilize the tissue. Slides were incubated with primary antibodies: anti-CD31 (1:100), anti-NG2 (1:100), anti-VE-cadherin (1:100), anti-ZO-1 (1:100) anti-claudin-5 (1:100), anti-angiopoietin-2 (1:100), anti-pTIE2 (1:100), and anti-connexin-43 (1:100) overnight at 4 °C, and then were washed with PBS three times and incubated with secondary antibodies (1:200–1:400) at room temperature for 1 h. After washing in PBS three more times, slides were mounted with VECTASHIELD Mounting medium with DAPI (Vector Laboratory) and photographed. HBMVECs were fixed in 4% PFA for 20 min, washed with PBS and permeabilized with 0.1% Triton X-100 for 2 min. After blocking for 30 min, primary and secondary antibodies were applied sequentially. Mounting and photography methods were the same as for tissue staining.

Fluorescence staining of whole-mount retinas. FITC-dextran perfused eyes from neonatal mice were collected on P5–P15 and fixed in 4% paraformaldehyde for 2 h on ice. For dissection, the cornea, lens, sclera and hyaloid vessels were removed. Retinas were permeabilized in 0.5% Triton/PBS (5% normal donkey serum) overnight at 4 °C, followed by incubation with primary antibodies diluted 1:50 in 0.1% Triton/PBS (1% normal donkey serum) overnight at 4 °C and then incubated with fluorescence secondary antibody overnight at 4 °C after washing. Retinas were then washed five times with PBS and mounted by making four incisions in fluorescence-mounting medium. Pictures were taken with the same exposure and gained using a confocal Leica TCS CP5 microscope (Leica, Germany). Vascular areas were outlined using NIH Image J software and quantified as the percentage of total area of retina analyzed.

Gene expression in tissue. Total RNA was isolated from tissues using the RNeasy kit with DNase I digestion (Qiagen, Valencia, CA). Reverse transcription (RT) was done by the standard procedure (Super Script first-strand synthesis system; Qiagen) using 1 µg of total RNA. Quantitative real-time polymerase chain reaction (qPCR) was performed using the iQ SYBR Green Supermix on iCycler real-time detection system (Bio-Rad Laboratories, Hercules, CA). RT–qPCR was performed with specific following mouse primers: *Gapdh* forward 5′-GCACAGTCAAGGCCGAGAAT-3′, *Gapdh* reverse 5′-GCCTTCTCCATGGTGGTGAA-3′; *Angpt1* forward 5′-ATTCTTCGCTGCCATTCT-3′, *Angpt1* reverse 5′-CAGTTCCCGTCGTGTTCT-3′; *Angpt2* forward 5′-TTCCTCTTGGGTGCTTTA-3′, *Angpt2* reverse 5′-CGCTTA TTTGGTGGTTATT-3′; *Tek* forward 5′-AGGGCAAGATGGATAGGG-3′, *Tek* reverse 5′-TGAGCACAGGGAGGGTTA-3′.

Cell culture. Mouse brain microvascular endothelial cells (MBMVECs) were isolated, as described previously[32]. The purity of the endothelial cells was verified by cell morphology, positive staining for VE-cadherin, von Willebrand factor, CD31 and VEGFR2, but negative staining for pericyte markers (SMA and NG2). Primary endothelial cells used for experiments were at passage three or fewer. *PDCD10* deletion in mouse endothelial cells was achieved by treatment with 4-hydroxyl tamoxifen (Sigma-Aldrich, H7904) at 100 nM; mock (DMSO/ethanol)-treated cells were used as a control. HBMVECs (cAP0002) and HBMVPCs (cAP-0030) were purchased from Angio-Proteomie (Boston). Endothelial cells were grown in Microvascular Endothelial Cell Growth Medium-2 MV (EGM2, Lonza) and HBMVPCs were grown in pericyte growth medium containing FBS and growth factor supplement (Angio-Proteomie). Human lung fibroblasts were routinely grown in DMEM supplemented with 10% FBS at 37 °C and 5% CO_2 and used between passages 10 to 14.

Lentiviral vector and packaging system. The Trans-Lentiviral Packaging System (Dharmacon) was used. The coding sequences for CCM3-WT (1–212 aa) and CCM3-N (a truncated CCM3 mutant containing the N-terminal 1–95 amino acids) were cloned into pLEX MCS vector (Clontech). Lentivirus expressing mCherry (rLV.EF1.mCherry-9) was purchased from Clontech. Plasmids were transfected and lentiviruses were produced and purified. Briefly, conditioned medium was harvested 62 h after transfection, cleared of debris by low-speed centrifugation, filtered through 0.45-µM filters (Falcon, Lincoln

Park, NJ) and assayed for transduction of HBMVECs by infecting cells overnight with serial dilutions of vector stock in culture medium supplemented with 8 µg/ml Polybrene (Sigma-Aldrich, St. Louis, MO). After medium replacement, the cells were further incubated for 36 h, and expression of RFP was scored by microscopy. The expression of CCM3-WT and of CCM3-N were determined by western blot. Concentrated vector stocks were prepared by ultracentrifugation of conditioned medium at 50,000g for 90 min. The pellet was resuspended in 0.05% of the starting volume in sterile PBS containing 4 µg/ml Polybrene. Stocks were titered as described above and stored frozen at −80 °C.

ANGPT2 ELISA. For measurements of ANGPT2 in human endothelial cell supernatant, the cells were treated and harvested at the indicated times. ELISA was performed with standard sandwich ELISA assay using anti-ANGPT2 antibodies from R&D, recombinant human ANGPT2 (625-AN-025), human ANGPT2 Mab (MAB098), human ANGPT2 biotinylated Mab (Bam0981). For measurement of ANGPT2 in mouse cells and tissues, the ANGPT2 mouse ELISA kits were from R&D (MANG20) and ABCAM (ab171335), respectively. For western blotting, mouse tissues were snap-frozen and tissues were homogenized in RIPA lysis buffer before undergoing SDS–PAGE. For ELISA, fresh mouse tissues were minced and then incubated in serum-free medium for 2 h. ANGPT2 protein in the supernatant was measured.

Real-time TIRF microscopy. TIRF imaging was performed using an IX-70 inverted microscope (Olympus), equipped with an argon (488-nm) laser line, a custom TIRFM condenser, a 60 × 1.45 NA TIRF objective (Olympus) and an EMCCD camera (iXon887; Andor Technology). The imaging system was controlled using iQ software (Andor Technology). For live-cell imaging, HBMVECs were seeded into 35-mm petri dishes with a no. 1.5 coverglass at the bottom of the wells (MatTek, Ashland, MA) in the EGM-2-MV culture medium (Lonza, cc-3202). The cells were first transfected with siCtrl (ThermoFisher, AM4636), siUNC13B (Santa Cruz, sc-42022), siCCM3 (Santa Cruz, sc-62084) or siCCM3 and siUNC13B using RNAiMAX (ThermoFisher). After 24 h, the cells were transfected with the VAMP8-PHluorin plasmid[24] using the Cytofect-Endothelial transfection kit (Cell Applications, TF101K). After another 24 h, time-lapse images of the transfected cells were acquired at 200-ms intervals at 37 °C in a custom incubation chamber. Stacks of time-lapse images were processed and analyzed using an algorithm within Image J 1.42 (National Institutes of Health) by a custom-written MATLAB program.

Transendothelial flux and TEER measurements. For transendothelial flux measurements, endothelial cells were seeded onto fibronectin-coated 96W20idf gold electrode ECIS cultureware (Applied BioPhysics) in EGM-2 medium (Lonza, cc-3202) and then transfected with siCtrl (ThermoFisher, AM4636), siUNC13B (Santa Cruz, sc-42022), siCCM3 (Santa Cruz, sc-62084) or siCCM3 and siUNC13B for 72 h. The barrier function of endothelial cells was assessed by electrical cell–substrate impedance sensing (Applied BioPhysics).

Organotypic angiogenesis assay. We employed a modified protocol for organotypic angiogenesis[37]. 8.5×10^3 HBMVECs with or without EGFP expression (infected by retrovirus (the Retro-X-System, Clontech); MOI 20) were transfected with siCtrl (ThermoFisher, AM4636), siUNC13B (Santa Cruz, sc-42022), siCCM3 (Santa Cruz, sc-62084) or siCCM3 and siUNC13B and then seeded onto confluent human fibroblasts that had been plated at 2×10^4 cells onto 24-well plates and grown to confluency over 7–14 d. Seeding was done at 48 h after endothelial cell infection or 24 h after transfection in EGM2, which was replenished every 2 d. Tubule formation was assessed 2–14 d after seeding by VE-cadherin and collagen IV staining or by visualization of EGFP-expressing endothelial cells grown on glass-bottom dishes (Mat Tek Corporation).

Three-dimensional bead-sprouting assay. MBMVECs were transfected with siCtrl, siUNC13B (Santa Cruz, sc-42022), siCCM3 (Santa Cruz, sc-62084) or siCCM3 and siUNC13B overnight by Lipofectamine RNAiMAX, following protocols provided by the manufacturer (Invitrogen), and changed to fresh prepared Microvascular Endothelial Cell Growth Medium-2 MV (EGM2, Lonza). The three-dimensional bead-sprouting assay was performed according to a published protocol[36]. Briefly, cells were harvested at 24 h post-transfection and were coated with Cytodex 3 microcarrier beads (C3275, Sigma-Aldrich) with a concentration of 400 cells per bead in EGM2 medium. These coated beads were embedded in 2 mg/ml fibrin gels in 24-well plates by mixing 2 mg/ml of fibrinogen (Calbiochem) in DPBS, 0.625 U/mL of thrombin (Sigma-Aldrich) and 0.15 U/ml of aprotinin (Sigma-Aldrich). EGM2 medium containing fibroblasts (20,000 per well) was added to each well with or without ANGPT2-neutralizing antibody (1 µg/ml or 10 µg/ml; Genentech). The cultures were maintained for 2–13 d by changing the medium every other day. Bright field images were captured with Axiovert 200 (Zeiss) at 10× magnification, and sprout lengths were measured with NIH ImageJ.

HBMVECs and HBMVPCs co-culture system in the 3D bead-sprouting assay. A spheroid sprouting assay for endothelial–pericyte interaction was performed. HBMVECs were infected with EGFP-expressing retrovirus and HBMVPCs were infected with mCherry-expressing lentiviruses (MOI 20). Endothelial cells were further transfected with siRNAs as indicated. Endothelial cells and pericytes (2:1) were seeded to onto Cytodex 3 microcarrier beads (Sigma-Aldrich) with a concentration of 400 cells per bead in Microvascular Endothelial Cell Growth Medium-2 MV (EGM2, Lonza). We chose a 2:1 ratio on the basis of our results showing that pericytes grow faster than endothelial cells and limited endothelial cell sprouting when at a 1:1 ratio (data not shown). These coated beads were embedded in fibrin gels as described above. EGM2 medium containing fibroblasts (20,000 per well) was added to each well with or without ANGPT2-neutralizing antibody (1 µg/ml or 10 µg/ml; Genentech). The cultures were maintained for 8 d by changing the medium every other day. Fluorescence images were captured with Axiovert 200 (Zeiss) at 10× magnification, and the percentages of pericyte coverage of endothelial tubes were measured with NIH ImageJ.

Study design and statistical analysis. Source data for the supplemental figures is available as **Supplementary Data Set 1**. Group sizes were determined by an *a priori* power analysis for a two-tailed, two-sample t test with an α of 0.05 and power of 0.8 to detect a 10% difference in lesion size at the endpoint. Animals were randomized into groups, and investigators were blinded to the groups of mice during the experiments. Male and female animals were used in equal numbers for all experiments. No samples or animals were excluded from analysis. All quantifications (lesion sizes, junctional integrity, sprout length and lumen) were performed in a blinded fashion. All figures are representative of at least three experiments unless otherwise noted. All graphs report mean ± s.e.m. values of biological replicates. Comparisons between two groups were performed by unpaired, two tailed t-test, between more than two groups by one-way ANOVA followed by Bonferroni's post-hoc or by two-way ANOVA using Prism 6.0 software (GraphPad). P values were two-tailed, and values < 0.05 were considered to indicate statistical significance. *$P < 0.05$, **$P < 0.01$ and ***$P < 0.001$ as designated in all figures.

List of antibodies. The following antibodies were used for immunostaining: angiopoietin-1 (goat, Abcam, ab133425, 1:200); angiopoietin-2 (goat, R&D, AF623, 1:100); angiopoietin-2 (rabbit, Abcam, ab8452, 1:200); angiopoietin-2 (rabbit, Novus, NBP2-1538, 1:100); β-vatenin (mouse, BD Pharmingen, 51 9001921, 1:100); CCM3 (mouse, Santa Cruz, SC365587, 1:1,000); CCM3 (rabbit, Min lab, 1:1,000); CD31 (rat, BD Pharmingen, 553370, 1:100); CD31 (rabbit, Abcam, ab28364, 1:100); claudin 5 (rabbit, Invitrogen, 34-1600, 1:100); collagen IV (rabbit, AbD Serotec, 2150-1470, 1:300); collagen IV (rabbit, Abcam, ab6586, 1:500); connexin 43 (mouse, BD Pharmingen, 51-9001918, 1:100); NG2 (rabbit, Millipore, AB5320, 1:100); phospho-TIE2(Tyr992) (rabbit, Cell Signaling, 4226, 1:1,000); phospho-Tie2 (Y992) (rabbit, R&D, AF2720, 1:100); TIE2 (rabbit, Cell Signaling, 4224, 1:1,000); VAMP3 (goat, Santa Cruz, sc-18208, 1:100); VE-cadherin (rat, BD Pharmingen, 555289, 1:100); VE-cadherin (goat, Santa Cruz, sc-6458, 1:100); ZO-1 (rabbit, Invitrogen, 61-7300, 1:100), Alexa Flour 488 Phalloidin (Invitrogen, A12379, 1:1,000); Alexa Fluor 594 Isolectin GS-IB4 conjugate (Invitrogen, I21413, 1:50); Alexa Fluor 488 donkey anti-rat IgG (Invitrogen, A21208, 1:200); Alexa Fluor 488 donkey anti-goat IgG (Invitrogen, A11055, 1:200); Alexa Flour 488 donkey anti-rabbit IgG (Invitrogen, A21206, 1:200); Alexa Fluor 488 donkey anti-mouse IgG (Invitrogen, A21202, 1:200); Alexa Fluor 594 donkey anti-rat IgG (Invitrogen, A21209, 1:200); Alexa Fluor 594 donkey anti-goat IgG (Invitrogen, A11058, 1:200); Alexa Fluor 594 donkey anti-rabbit IgG (Invitrogen, A21207, 1:200); Alexa Fluor 594 donkey anti-mouse IgG (Invitrogen, A21203, 1:200).

The following antibodies were used for western blot: rabbit polyclonal antibody against CCM3 was generated (Invitrogen) against full-length recombinant human CCM3 protein expressed and purified from *Escherichia coli*. β-actin is from Sigma-Aldrich (mouse, A1978); GAPDH (rabbit, 2118), p-Smad2 (rabbit, 3180), p-MLC (rabbit, 3674), VEGFR2 (rabbit, 2479), p-TIE2 (rabbit, 4221), TIE2 (rabbit, 4224), p-FAK (rabbit, 3281) are from Cell Signaling Technology; β-catenin (mouse, sc-7963), CDC42 (mouse, sc-8401), RAC1 (sc-217), RhoA (mouse, sc-418), STK25 (goat, sc-6865) and VAMP-3 (goat, sc-18208) are from Santa Cruz Biotechnology. ANGPT2 (rabbit, Ab8452) is from Abcam and ANGPT2 (AF7186) from R&D; integrin-β1 (mouse, 610467) and FAK (mouse, 610087) are from BD. All primary antibodies were used at 1:1,000 dilution.

60. Li, S. *et al.* Retro-orbital injection of FITC-dextran is an effective and economical method for observing mouse retinal vessels. *Mol. Vis.* **17**, 3566–3573 (2011).

ERRATA

Erratum: Endothelial exocytosis of angiopoietin-2 resulting from CCM3 deficiency contributes to cerebral cavernous malformation

Huanjiao Jenny Zhou, Lingfeng Qin, Haifeng Zhang, Wenwen Tang, Weidong Ji, Yun He, Xiaoling Liang, Zongren Wang, Qianying Yuan, Alexander Vortmeyer, Derek Toomre, Germaine Fuh, Minghong Yan, Martin S Kluger, Dianqing Wu & Wang Min

In the version of this article initially published, labels for micrographs in Figure 2d and Figure 5b were omitted, and two grants were not acknowledged in the Acknowledgments section. The errors have been corrected in the HTML and PDF versions of the article.